

Modeling Elasticity in Crystal Growth

K. R. Elder¹, Mark Katakowski¹, Mikko Haataja² and Martin Grant².

¹*Department of Physics, Oakland University, Rochester, MI, 48309-4487*

²*Physics Department, Rutherford Building, 3600 rue University, McGill University, Montréal, Québec, Canada H3A 2T8.*

(October 27, 2018)

A new model of crystal growth is presented that describes the phenomena on atomic length and diffusive time scales. The former incorporates elastic and plastic deformation in a natural manner, and the latter enables access to times scales much larger than conventional atomic methods. The model is shown to be consistent with the predictions of Read and Shockley for grain boundary energy, and Matthews and Blakeslee for misfit dislocations in epitaxial growth.

05.70.Ln, 64.60.My, 64.60.Cn, 81.30.Hd

The appearance and growth of crystal phases occurs in many technologically important processes including epitaxial growth and zone refinement. While a plethora of models have been constructed to examine various aspects of these phenomena it has proved difficult to develop a computationally efficient model that can be used for a wide range of applications. For example, standard molecular dynamics simulations include the necessary physics but are limited by atomic sizes (Å) and phonon time scales (ps). Conversely continuum field theories can access longer length (i.e., correlation length) and time (i.e., diffusive) scales, but are difficult to incorporate with the appropriate physics. In this paper a new model is presented that includes the essential physics and is not limited by atomic time scales.

To illustrate the features that must be incorporated it is useful to consider two examples. First consider the nucleation and growth of crystals from a pure supercooled liquid or vapor phase. In such a process small crystallites nucleate (heterogeneously or homogeneously) and grow in arbitrary locations and orientations. Eventually the crystallites impinge on one another and grain boundaries are formed. Further growth is then determined by the evolution of grain boundaries. Now consider the growth of a thin crystal film on a substrate of a different crystal structure. Typically the substrate stresses the over-lying film which can destabilize the growing film and cause an elastic defect-free morphological deformation [1,2], plastic deformation involving misfit dislocations [3], or a combination of both. Thus the model must be able to nucleate crystallites at arbitrary locations and orientations and contain elastic and plastic deformations. While all these features are naturally incorporated in atomistic descriptions, they are much more difficult to include in continuum or phase field models.

Historically, many continuum models have been developed to describe certain aspects of crystal growth and liquid/solid transitions in general. At the simplest level, ‘model A’ in the Halperin and Hohenberg [4] classification scheme has been used to describe liquid/solid transitions. This model treats all solids equivalently and does not introduce any crystal anisotropy. Extensions to this basic model have been developed to incorporate a solid

phase that has multiple states that represent multiple orientations [5,6] or recently [7] an infinite number of orientations. Unfortunately these models do not properly include plastic and elastic deformations. Other models [8–12] have sought to include elastic and plastic deformations with reference to a specific reference lattice, but cannot account for multiple orientations.

In this work these limitations are overcome by considering a free energy that is minimized by a periodic hexagonal (i.e., solid) state. Such free energies have arisen in many other physical systems [13,14] (such as water/surfactant systems, copolymers, Rayleigh-Bénard convection and ferromagnetic films) and in some instances have even been described in terms of crystalline terminology [14]. The model used in this work describes the statics and dynamics of a conserved field, ψ , by the following free energy and equation of motion,

$$\mathcal{F} = \int d\vec{r} (\psi [(q_o^2 + \nabla^2)^2 - \epsilon] \psi/2 + \psi^4/4) \quad (1)$$

and

$$\partial\psi/\partial t = \nabla^2 (\delta\mathcal{F}/\delta\psi) + \eta, \quad (2)$$

where η is a stochastic noise, with zero mean and correlations $\langle \eta(\vec{r}, t) \eta(\vec{r}', t') \rangle = -G \nabla^2 \delta(\vec{r} - \vec{r}') \delta(t - t')$, and $G = 0$ hereafter, q_o and ϵ are constants. The field ψ represents the average atomic positions. The focus of this paper is on two dimensions (2D); it is straightforward to extend these calculations to 3D. In two dimensions, this free energy is minimized by striped (ψ_s), hexagonal (ψ_h) and constant (ψ_c) states depending on the average value, $\bar{\psi}$, of ψ . To estimate the phase diagram these states can be approximated $\psi_s = A_s \sin(q_s x) + \bar{\psi}$

$$\psi_h = A_h \left[\cos(q_h x) \cos\left(\frac{q_h y}{\sqrt{3}}\right) + \frac{1}{2} \cos\left(\frac{2q_h y}{\sqrt{3}}\right) \right] + \bar{\psi} \quad (3)$$

and $\psi_c = \bar{\psi}$. Substituting these expressions into Eq. (1) and minimizing subject to the constraint $\int d\vec{r} \psi = \bar{\psi}$ gives the values for the characteristic amplitudes A and

wavenumber q [15] and the phase diagram show in Fig. (1a).

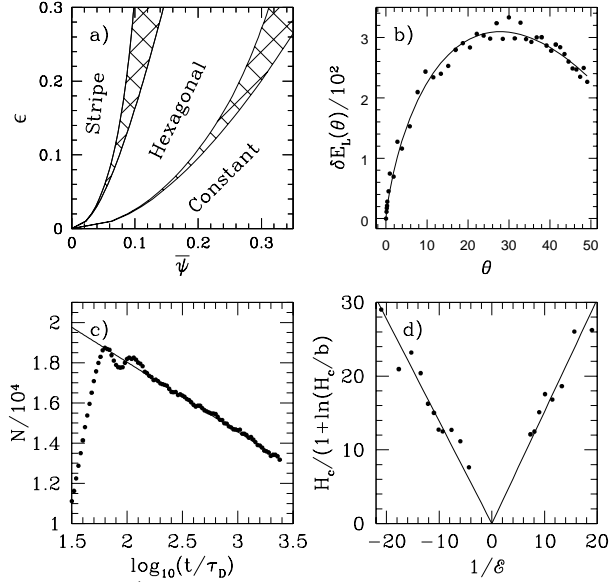


FIG. 1. a) Mean field phase diagram. In this figure the ‘hatched’ regions are coexistence regions. b) Grain boundary energy. The points are from numerical simulations and the line a fit to the Read-Shockley equation. c) Grain growth. In this figure the number defects is plotted and the solid line is a guide to the eye. d) Epitaxial growth. The points are from numerical simulations and the lines are best fits.

The linear elastic properties of the hexagonal phase can be determined by calculating the change of energy under shear, bulk or dilational deformations within the two mode approximation given in Eq. (3). It is straightforward to find the elastic moduli for the isotropic solid: $C_{12} = C_{44} = C_{11}/3$, where

$$C_{12} = \left[\left(3\bar{\psi} + \sqrt{15\epsilon - 36\bar{\psi}^2} \right) q_o^2 \right]^2 / 75. \quad (4)$$

For these coefficients [18] the Poisson ratio is $\nu = 1/3$ and the shear modulus is $\mu = C_{12}$.

The energy per unit surface length, E_L , between grains that differ in orientation by an angle θ was determined numerically and, in Fig. (1b), compared with the prediction of Read and Shockley [17], i.e., $E_L = E_M \theta [1 - \ln(\theta/\theta_M)]$ where E_M and θ_M are constants. The parameters of the simulations were $(\epsilon, \bar{\psi}, q_o) = (4/15, 1/4, 1)$. In all the simulations conducted in the paper the time and space size were $\Delta t = 0.01$ and $\Delta x = \pi/4$ respectively. The Read-Shockley form closely fits the data for $\theta_M = 27.85^\circ$ and $E_M = 0.064$. The maximum angle, θ_M is similar to those observed in experiment [17]. The maximum energy/length, E_M , can be estimated using the Read-Shockley equation [17] in 2D [18] using the elastic constants estimated above, $E_M = \mu(1 + \nu)b/4\pi = C_{12}b/3\pi$, where $b = 2\pi/q_h$ is the magnitude of the Burger’s vec-

tor. For the parameters used in the simulations this gives $E_M = 0.044$, as compared to our measured value of 0.064.

The main advantage of the current approach over molecular dynamics simulations is the time scales that are accessible. To illustrate this point it is useful to calculate the diffusion time using a standard Block-Floquet linear analysis. In such an approach the dynamics of a perturbation ($\delta\psi$) around an equilibrium crystal state (ψ_{eq}) is obtained by first substituting $\psi = \delta\psi + \psi_{eq}$ into Eq. (2) and linearizing in $\delta\psi$. Substituting appropriate forms for the equilibrium state (i.e., $\psi_{eq} = \psi + \sum a_{n,m} \exp[i(nq_x x + mq_y y)]$) and perturbation along one of the three principle axes (i.e., $\delta\psi = \sum \delta a_{n,m}(t) \exp[i(n(q_x + Q)x + mq_y y)]$) and integrating over $\exp[i(kq_x x + lq_y y)]$ gives an equation of motion for the modes $\delta a_{n,m}$. Using the approximation for ψ_{eq} given in Eq. (3) and four modes (i.e., $(\delta a_{1,1}, \delta a_{-1,1}, \delta a_{1,-1}, \delta a_{-1,-1})$) to describe the perturbation leads to a set of four linear ordinary differential equations that can be solved analytically, assuming $\delta a_{n,m} \sim \exp(\omega t)$. The largest eigenvalue is equal to $\omega = -3q_o^4 Q^2$ implying a diffusion constant of $3q_o^4$. In terms of times steps, this implies it takes roughly 1000 times steps for a diffusion time, τ_D [16], for the simulation parameters used in this paper.

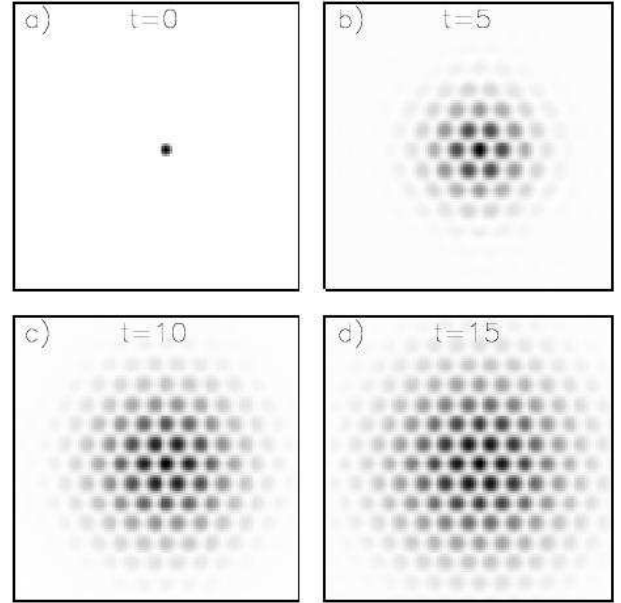


FIG. 2. Vacancy diffusion. In this plot the gray scale is proportional to the difference between a perfect lattice and the one containing the vacancy at times $t/\tau_D = 0, 5, 10$ and 15 in a), b), c), and d) respectively. For clarity the magnitude of the gray scale was maximized in each figure.

To confirm these calculations, vacancy diffusion was studied numerically by removing a single ‘particle’ from a perfect hexagonal lattice, for the parameters used in the grain boundary simulations. The dynamics of a vacancy is depicted in Fig. (2). It is important to note that this model describes long times scales so the vacancy does not

‘jump’ from site to site, but the probability of finding the vacancy diffuses into the background matrix as shown in Fig. (2). The rate of spread can be used to numerically determine the diffusion constant and was $D = 2.96$ which is quite close to the approximate calculation (i.e., $D = 3$, for $q_o = 1$).

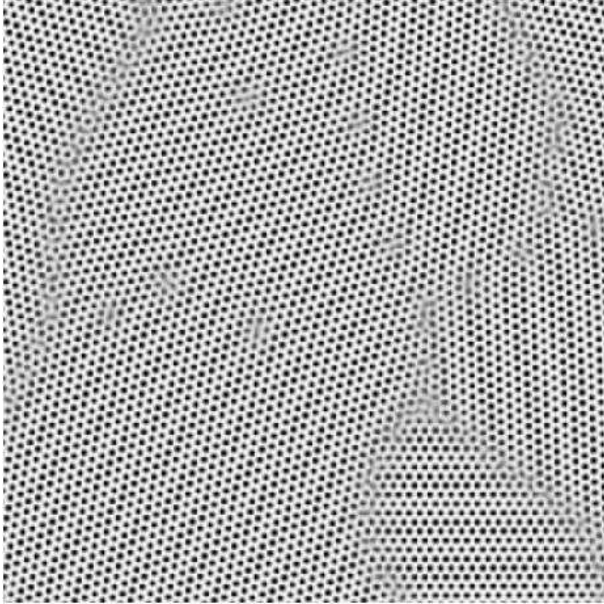


FIG. 3. Grain Growth. Gray scale plot of the order parameter ψ at $t/\tau_D = 700$. This plot contains one sixty-fourth of the full simulations cell.

The ability of the continuum model to describe multiple crystals in arbitrary orientations and locations with the appropriate grain boundaries energies on diffusive time scales makes it ideal for the study of grain boundary growth. To study this phenomena a system of size $4096\Delta x \times 4096\Delta x$ was simulated with parameters $(\epsilon, \bar{\psi}, q_o) = (0.1, 0.05, 1)$. To begin the simulations, 256 crystals were nucleated at arbitrary locations by placing large fluctuations in ψ at each nucleation site. As time evolves the small crystallites grow from the initial seeds until impingement. Eventually the entire systems is filled with the hexagonal phase and further evolution continues by motion at grain boundaries. At this stage in the simulations there were approximately 236,000 particles. To study the subsequent dynamics the number defects, where a defect is defined as a particle that does not have six nearest neighbors, was monitored. The number of defects is shown in Fig. (1c) as a function of the logarithm of time. Initially ($\log(t) < 1.7$) the number of defect increases as the total droplet surface area increases. When the droplets impinge, the number of defects begins to decrease as local rearrangements take place. At later times ($\log(t/\tau_D) > 2.0$) the grain boundaries evolve at a very slow rate. In these simulations it is found that the number of defects decreases logarithmically at late times.

The inclusion of elastic and plastic deformations allow the study of morphological instabilities in epitaxial

growth. When a film grows on a bulk material that has a different lattice constant the film can become corrugated (“buckle”) in an attempt to relieve the strain [1]. The buckling of the surface relieves the strain in some regions but increases the strain in others. At these locations dislocations eventually nucleate. The critical height, H_c , at which these nucleate is well described by the Matthews and Blakeslee equation [3] which has the functional form, $H_c = H_o[1 + \ln(H_c/b)]/\mathcal{E}$, where H_o is a constant and \mathcal{E} is the mismatch between the film and bulk lattice parameters, i.e., $\mathcal{E} = (a_{film} - a_{bulk})/a_{bulk}$, where a is a lattice constant.

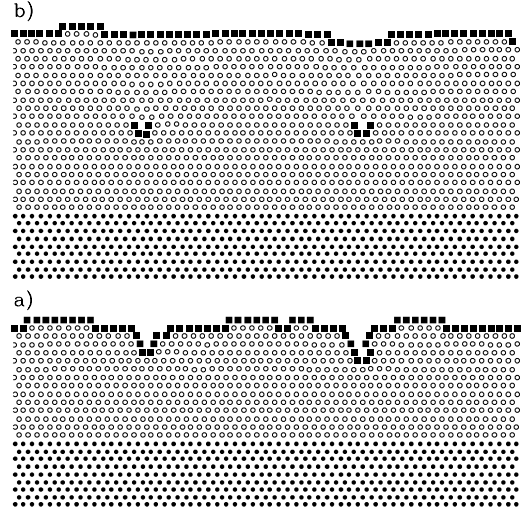


FIG. 4. Epitaxial Growth. In this figure the film and bulk particles (defined as local maxima of ψ) are plotted as open and closed circles respectively. Defects are plotted as solid squares.

To study this phenomena a thin film with $q_o = q_f$ was grown on a bulk sample ($q_o = 1$) with the parameters $(\epsilon, \bar{\psi}) = (1/4, 1/4)$ for various values of q_f . The system had a width of $8192\Delta x$ and height $1024\Delta x$. A small portion of a sample simulation is shown in Fig. (4) for a lattice mismatch of 6.4% , (i.e., $\mathcal{E} = (2\pi/q_f - 2\pi/q_o)/(2\pi/q_o) = 0.064$). The buckling phenomena is shown in Fig. (4a) and the nucleation of dislocations in Fig. (4b). The critical height was defined as the height at which the interface velocity changes (i.e., since the number of particles arriving at the surface is conserved the velocity of the film interface changes when dislocations appear and change the total number of interface particles). The numerical results for H_c shown in Fig. (1d) are consistent with the functional relationship proposed by Matthews and Blakeslee [3].

The one component model described by Eqs. (1) and (2) does not support other metastable crystal phases and thus cannot be used to, for example, study structural phase transitions. However it is straightforward to ex-

tend the model to include more than one kind of particle which can give rise to other metastable crystal phases. For example a binary system can be easily modeled by a free energy of the form;

$$\mathcal{F} = \int d\vec{r} \left(\psi_1 [(q_1^2 + \nabla^2)^2 - \epsilon_1] \psi_1/2 + \psi_1^4/4 + \psi_2 [(q_2^2 + \nabla^2)^2 - \epsilon_2] \psi_2/2 + \psi_2^4/4 + \alpha \psi_1 \psi_2 \right) \quad (5)$$

and the equations of motion; $\partial\psi_1/\partial t = \Gamma_1 \nabla^2 \delta\mathcal{F}/\delta\psi_1 + \eta_1$ and $\partial\psi_2/\partial t = \Gamma_2 \nabla^2 \delta\mathcal{F}/\delta\psi_2 + \eta_2$, where α is a coupling constant. The properties (i.e., lattice constant, bulk compressibility, etc.) of the individual atoms are controlled by the parameters with subscripts 1 or 2 and by the average value of ψ_1 and ψ_2 . When an individual binary alloy droplet is grown a hexagonal pattern typically emerges. However when a random initial condition is used the patterns usually contain more than one crystal phase since the energy of the hexagonal state is very close to a face centered cubic. One such a configuration is shown in Fig. (5). Eventually the system will evolve to a hexagonal state. Thus the model can be used to study structural phase transitions.

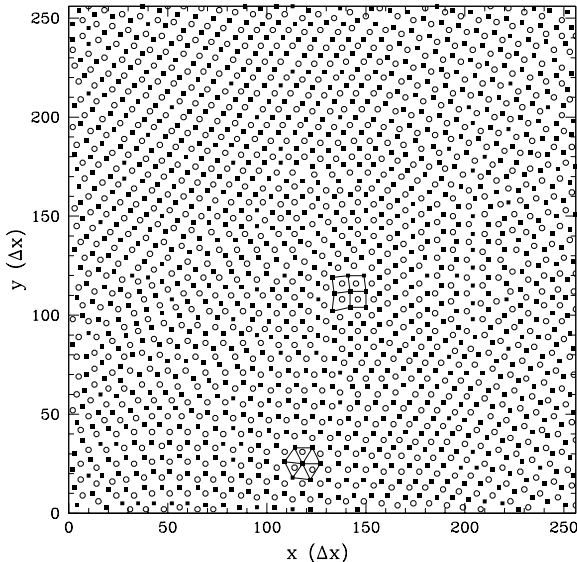


FIG. 5. Binary Alloy. In this figure the open circles and solid squares are the maxima of ψ_1 and ψ_2 respectively. Two different crystal structures have been highlighted by joining nearest neighbors of the same species.

In conclusion, the preceding simulations and calculations have provided ample evidence that the model described by Eqs. (1) and (2) provide an adequate description of crystal behavior on long time and atomic length scales. Thus this model should provide a useful method of studying the crystallization of pure and multicomponent materials.

This work was supported by a Research Corporation grant CC4787 (KRE), and a NSF-DMR Grant 0076054

(KRE), the Academy of Finland (MH), the Natural Sciences and Engineering Research Council of Canada (MG) and *le Fonds pour la Formation de Chercheurs et l'Aide à la Recherche du Québec* (MG),

-
- [1] R. J. Asaro and W. A. Tiller, *Metall. Trans.* **3**, 1789 (1972).
 - [2] M. Grinfeld, *Dokl. Akad. Nauk. SSSR* **265**, 836 (1982); *Europhys. Lett.* **22**, 723 (1993).
 - [3] J. W. Matthews and A. E. Blakeslee, *J. Cryst. Growth* **27**, 118 (1974). J. W. Matthews, *J. Vac. Sci. Technol.* **12** 126 (1975).
 - [4] P. C. Hohenberg and B. I. Halperin, *Rev. Mod. Phys.* **49**, 435 (1977).
 - [5] B. Morin, K. R. Elder, M. Sutton and M. Grant, *Phys. Rev. Lett.* **75**, 2156 (1995).
 - [6] L.-Q. Chen and Wang, *Phys. Rev. B* **50**, 15752 (1994).
 - [7] J. A. Warren, W. C. Carter, and R. Kobayashi, *Physica A* **261**, 159 (1998); J. A. Warren, R. Kobayashi and W. C. Carter, *J. Cryst. Growth* **211**, 18 (2000); R. Kobayashi, J. A. Warren and W. C. Carter, *Physica D* **140**, 141 (2000).
 - [8] J. Müller and M. Grant, *Phys. Rev. Lett.* **82**, 1736 (1999). M. Haataja, J. Müller, A. D. Rutenberg, and M. Grant (preprint).
 - [9] D. Orlikowski, C. Sagui, A. Somoza, and C. Roland, *Phys. Rev. B* **59**, 8646 (1999).
 - [10] A. E. Jacobs, *Phys. Rev. B* **61**, 6587 (2000).
 - [11] M. Sanati, A. Saxena, T. Lookman, and R. C. Albers, *Phys. Rev. B* **63**, 224114 (2001).
 - [12] Y. U. Wang, Y. M. Jin, A. M. Cuitiño, and A. G. Khachaturyan, *App. Phys. Lett.* **78**, 2324 (2001).
 - [13] A. Linhananta and D. E. Sullivan, *Phys. Rev. E* **57**, 4547 (1998); I. I. Potemkin and S. V. Panyukov, *Phys. Rev. E* **57**, 6902 (1998); J. Swift and P. C. Hohenberg, *Phys. Rev. A* **15**, 319 (1977).
 - [14] C. Sagui and R. C. Desai, *Phys. Rev. E* **52**, 2807 (1995)
 - [15] In this approximation the free energy is minimized when $A_s = 2\sqrt{3\epsilon - 9\bar{\psi}^2}/3$, $q_s = q_o$, $A_h = -4(b + \sqrt{15\epsilon - 36\bar{\psi}^2}/3)/5$ and $q_h = \sqrt{3}q_o/2$.
 - [16] In this paper a diffusion time, τ_D is defined as the time for a particle to diffuse one lattice constant and is equal to a^2/D where a is the lattice constant, i.e., $a \approx 2\pi/(\sqrt{3}q_o/2)$.
 - [17] W. T. Read and W. Shockley, *Phys. Rev.* **78**, 275 (1950).
 - [18] See, for example: *Principles of condensed matter physics*, P. M. Chaikin and T. C. Lubensky (Cambridge University Press, Cambridge, 1995); *Theory of elasticity, 3rd edition* and L. D. Landau and E. M. Lifshitz (Butterworth-Heinemann, Oxford, 1998).